Supporting Information

Molecular Structure Design of Planar Zwitterionic Polymer Electrode Materials for All-Organic Symmetric Battery

Jun Wang,[a] Haichao Liu,[c] Chunya Du,[c] Yu Liu,[d] Bing Liu[a], Haoran Guan[a], Shaowei Guan,*[a] Zhenhua Sun*[b] and Hongyan Yao *[a]

[a.] *National & Local Joint Engineering Laboratory for Synthesis Technology of High Performance Polymer, Key Laboratory of High Performance Plastics, Ministry of Education, College of Chemistry, Jilin University, Qianjin Street 2699, Changchun, 130012, P. R. China.*

[b.] *Shenyang National Laboratory for Materials Science, Institute of Metal Research, Chinese Academy of Sciences, Shenyang 110016, P. R. China.*

[c.] *State Key Lab of Supramolecular Structure and Materials, Jilin University, 2699 Qianjin Avenue, Changchun, 130012, P. R. China.*

[d.] *College of Sciences, Shenyang University of Chemical Technology, Shenyang, 110142, P. R. China.*

Table of Contents

Experimental Procedures

Materials

All materials, including squaric acid (SQ), 2,6-diaminoanthraquinone (2,6-DAQ) and solvents, were purchased from commercial resources and used as received without further purification. All compounds are >95% pure by HPLC.

Synthesis of PSQ

Typically, squaric acid (3.42 g, 30 mmol) and 2,6-diaminoanthraquinone (10.71 g, 30 mmol) were added to n-butanol/o-dichlorobenzene (600 mL, 5:1 in vol.), and the mixture was stirred under reflux under a nitrogen environment for 24 h. The resultant reactant mixture was filtered and washed with THF and DMF for three times. The obtained dark red powder was dried at 100 °C under vacuum for 12 h. The obtained product is denoted as PSQ. PSQ is insoluble in common organic solvents including NMP, DMF, THF, DMAc, DOL and DME. Yield: 92%. Anal. Calcd. for PSQ $(C_{18}H_8N_2O_4)_n$: C 68.36, H 2.55, N 8.86%; Found: C 64.52, H 4.07, N 8.25%.

Synthesis of PSQ-K

PSQ-K was synthesized as an optimization sample to show the full redox potential of PSQ as cathode material. The corresponding synthesis route is similar to that of PSQ, except the addition of Ketjenblack before the polymerization process. The amount of Ketjenblack was determined according the yield of PSQ and controlled as 80% of the amount of PSQ.

Instrumental Characterization

Solid-state ^{13}C nuclear magnetic resonance (^{13}C NMR) was performed on a Bruker AVANCE III 400 WB solid 400 megabyte (wide cavity) superconducting NMR spectrometer. Fourier transform infrared (FT-IR) spectroscopy was recorded on Nicolet Impact 410 Fourier-transform infrared spectrometer. Elemental analysis (EA) was performed on a Vario Micro Cube Elemental Analyzer. X-ray photoelectron spectroscopy (XPS) was performed on an ESCA LAB MARK II spectrometer. Thermal gravimetric analysis (TGA) was performed on a PerkinElmer TGA-7 thermogravimetric analyzer over the temperature range of 100-800 °C under an N_2 atmosphere at a heating rate of 10 °C/min. X-ray diffraction (XRD) analysis was conducted on a Rigaku D/MAX-2550 diffractometer. The morphology of the samples was explored by field-emission scanning electron microscopy (FE-SEM, SU8020 model HITACHI microscope) and transmission electron microscopy (TEM, JEOL model JEM-2100 microscope). The optimized geometries and frontier molecular orbitals were obtained by using the Gaussian 09 (version D.01) package on a PowerLeader cluster, and density functional theory (DFT) was applied at the level of B3LYP/6-31G(d, p). The molecular electrostatic potential (MESP) was obtained by using Multiwfn Software.[59]

Cell assembly and electrochemical measurements

The organic cathode was prepared by mixing PSQ with super p and PVDF in N-methyl-2-pyrrolidone (NMP) with a weight ratio of 5:4:1. The organic anode was prepared by mixing PSQ with super p and sodium alginate in H_2O with a weight ratio of 5:4:1. The PSQ-K electrode was prepared by mixing PSQ-K with PVDF in NMP with a weight ratio of 9:1. They were dried under vacuum at 120 °C and 60 °C for 10 h for the cathode and anode, respectively. The corresponding average mass loading is ca. 1 mg cm^{-2}. The half batteries were assembled in a glove box (H_2O and O_2 concentrations < 0.01 ppm) using a CR2032 coin cell, in which metallic lithium was used as the counter electrode, Celgard 2400 was used as the separator, and Al and Cu were used as the current collectors for the cathode and anode, respectively. A solution of 1 M LiTFSI in 1,3-dioxane (DOL) and dimethoxyethane (DME) (1:1, v/v), and 1 M $LiPF_6$ in ethylene carbonate (EC): diethyl carbonate (DEC) (1: 1 v/v) were used as electrolyte for the cathode and anode, respectively. About 100 μL electrolyte was used in each cell. The all-organic symmetric batteries were assembled using PSQ cathode and prelithiated PSQ anode. The electrolyte is 1 M LiTFSI in 1,3-dioxane (DOL) and dimethoxyethane (DME) (1:1, v/v), and the ratio of mass loading of the cathode and anode is optimized as ca. 3:1. The capacity is determined based on the mass of the cathode.

Galvanostatic charge-discharge experiments were conducted in the voltage window of 1.0-3.5 V (vs. Li$^+$/Li) for the cathode, 0.01-3.0 V (vs. Li$^+$/Li) for the anode and 0.1-3.0 V for all-organic symmetric battery using a battery test system (CT2001A, Land). Cyclic voltammetry (CV) at various current densities and electrochemical impedance spectroscopy (EIS, 0.1 Hz–100 kHz frequency range) measurements were recorded on a CHI600C electrochemical workstation.

For the ex-situ FT-IR and XPS tests, the corresponding batteries at different charge-discharge states were disassembled in an argon-filled glove box and washed with dimethoxyethane (DME) several times to remove the electrolyte. The electrodes were dried under vacuum at room temperature before the measurements.
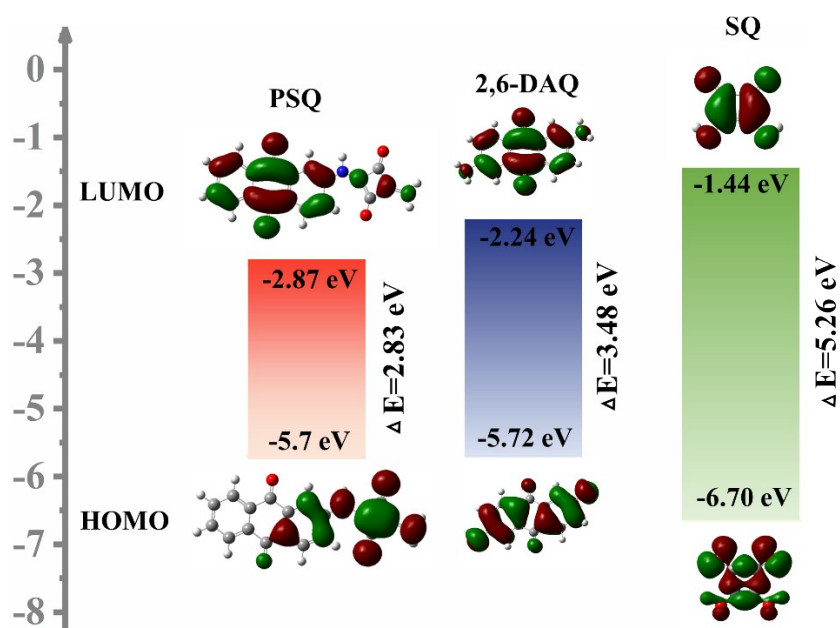
Figure S1. Calculated LUMO and HOMO energies for PSQ (repeat unit = 1) and monomers.

Figure S2. Photos of PSQ obtained from a one-pot polymerization process (the mass of PSQ is ca. 4 g, yield 92%).
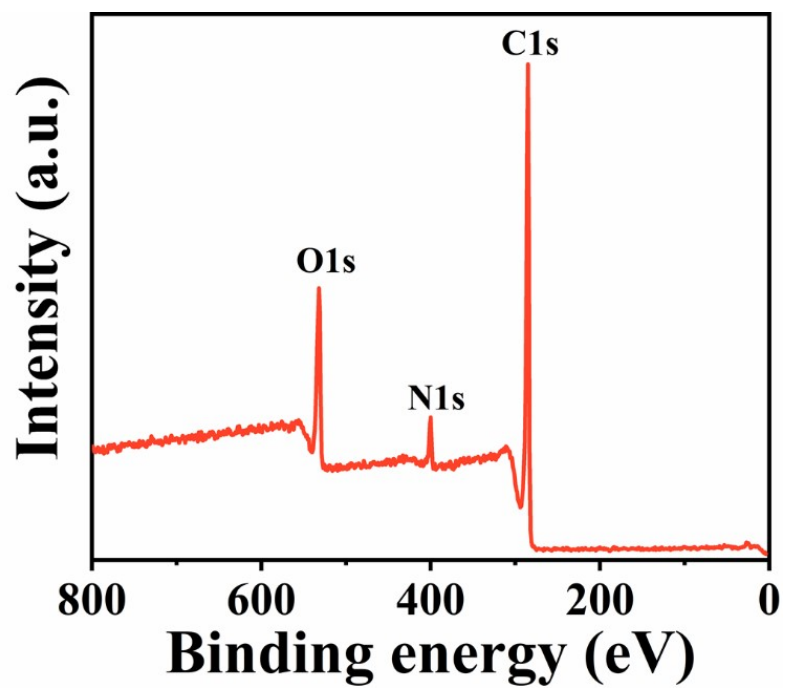
Figure S3. XPS pattern of PSQ.
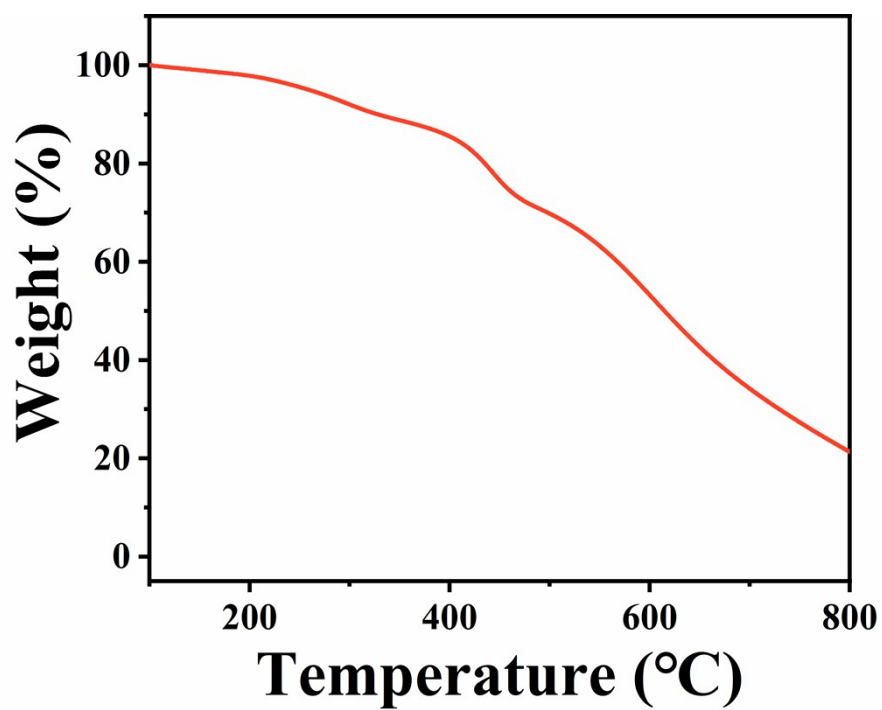
Figure S4. TGA curve of PSQ.
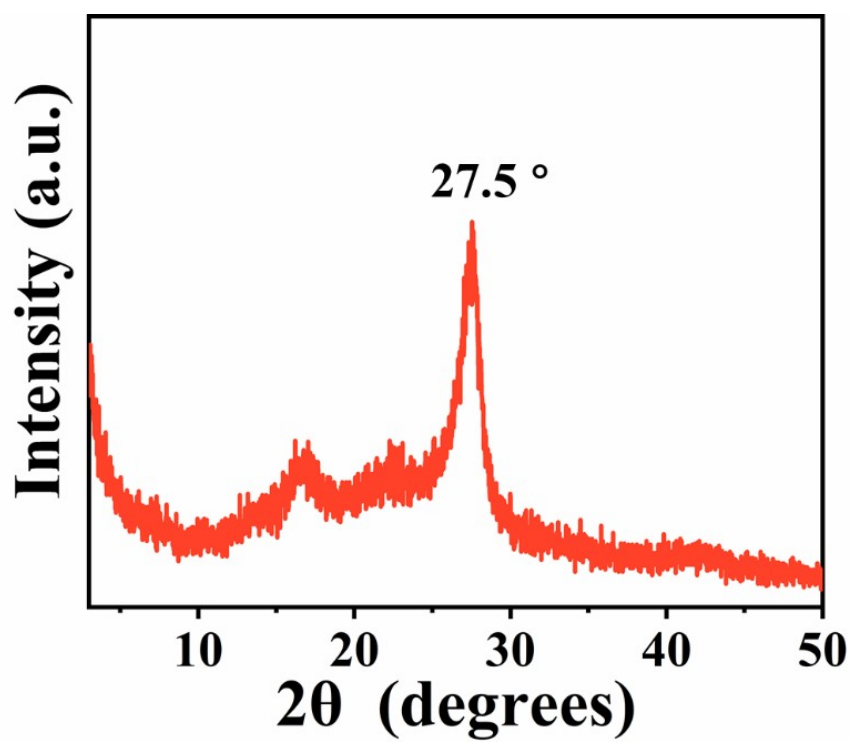
Figure S5. XRD pattern of PSQ.
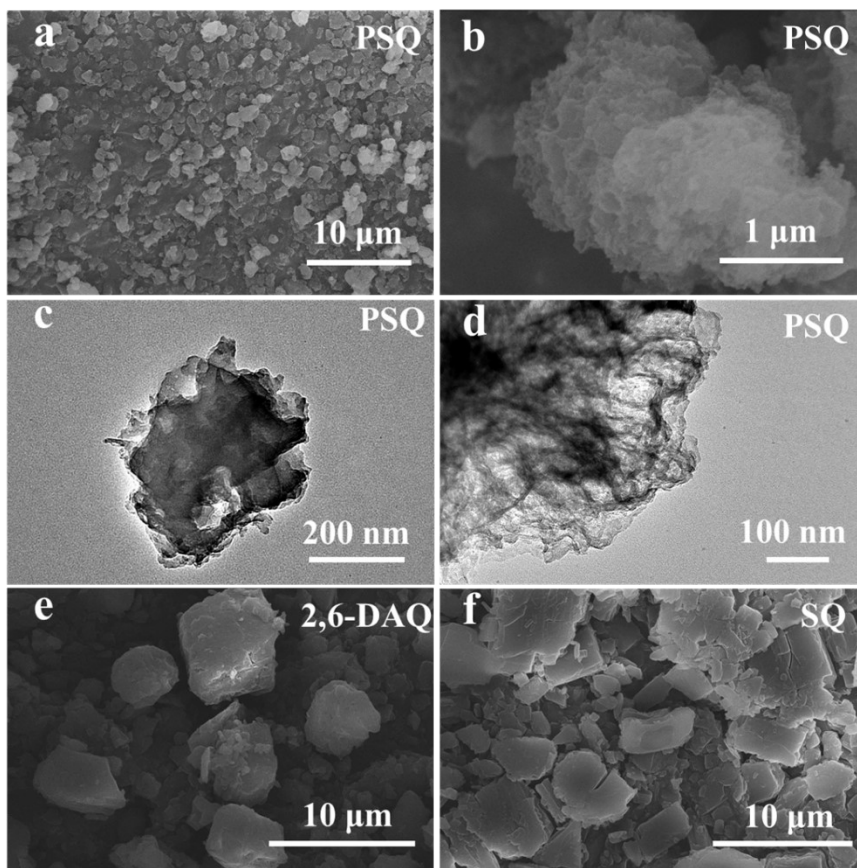
Figure S6. (a, b) SEM images of PSQ. (c, d) TEM images of PSQ. (e, f) SEM images of monomers.
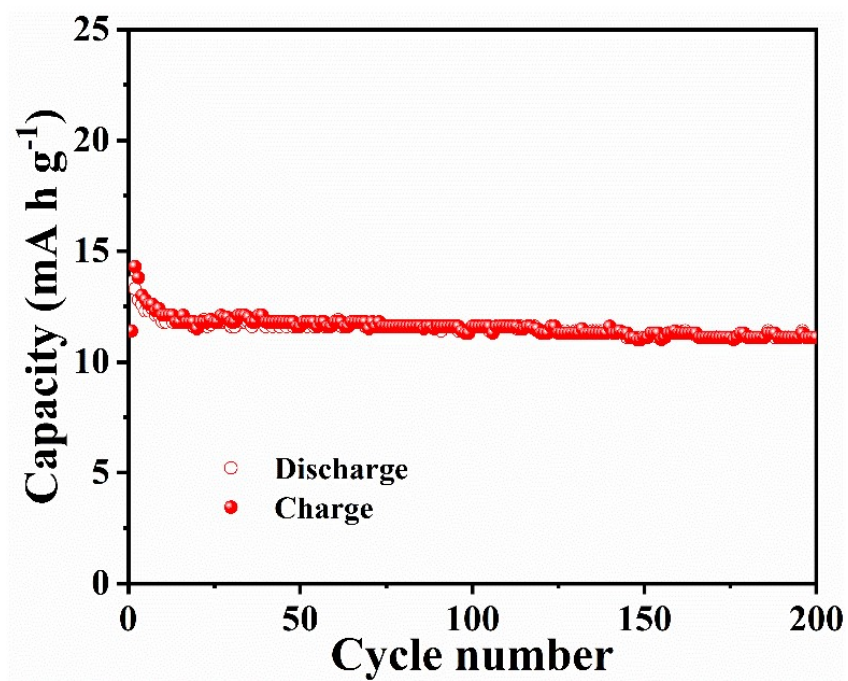
Figure S7. Cycling performance of conductive carbon in the PSQ cathode at 100 mA g^{-1}. (The capacity contribution of conductive carbon is lower than 5 mAh g^{-1}).
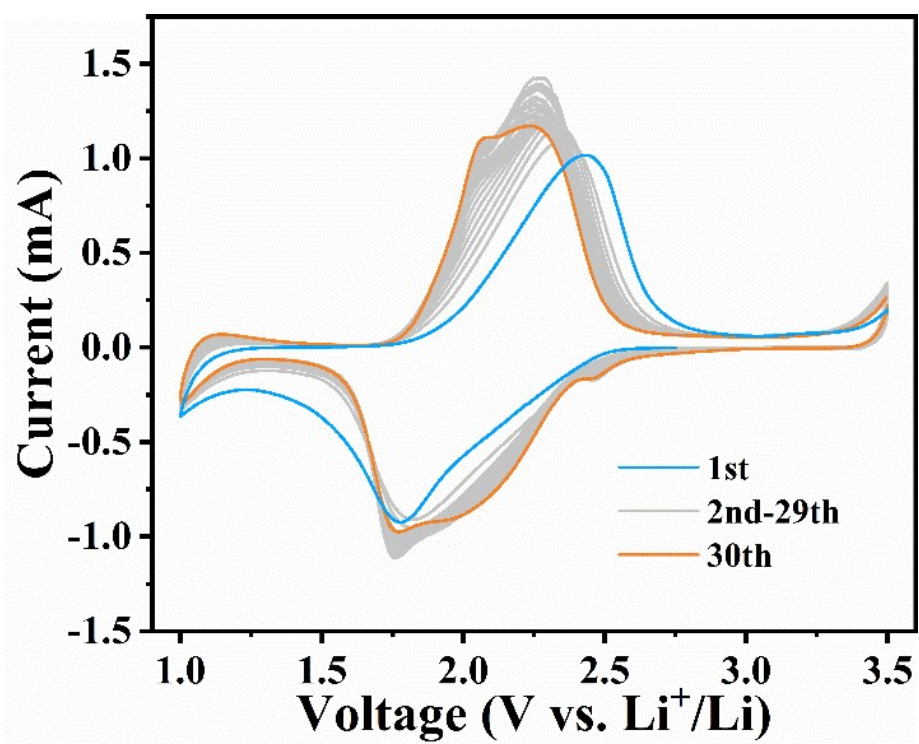
Figure S8. CV curves of the PSQ cathode at 2 mVs^{-1}.
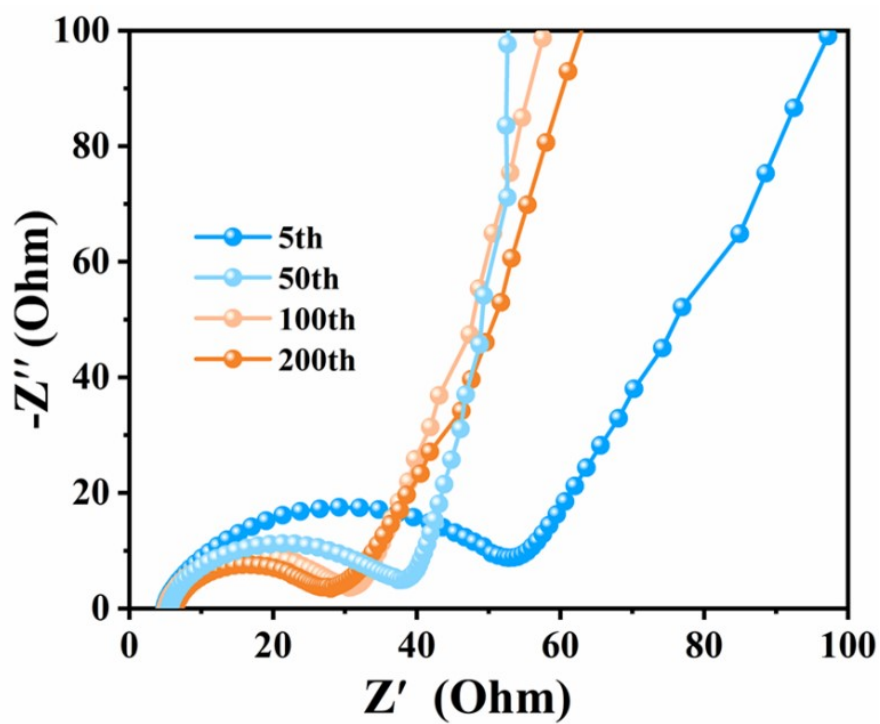
Figure S9. The Nyquist plot of the PSQ cathode at different cycle numbers at 100 mA g^{-1}.
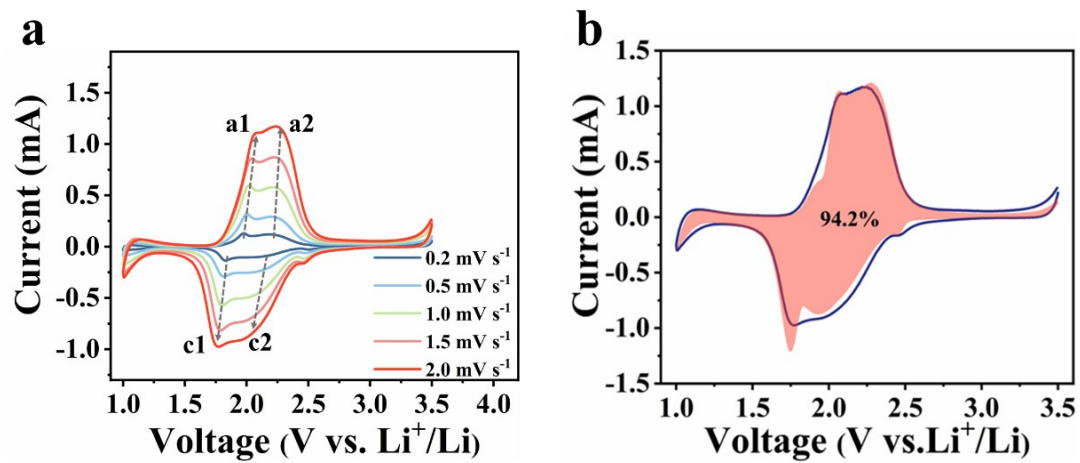
Figure S10. (a) CV curves of PSQ cathode at various scan rates from 0.2 to 2 mV s^{-1}. (b) Surface and diffusion-controlled contributions of the PSQ cathode at 2 mVs^{-1}.
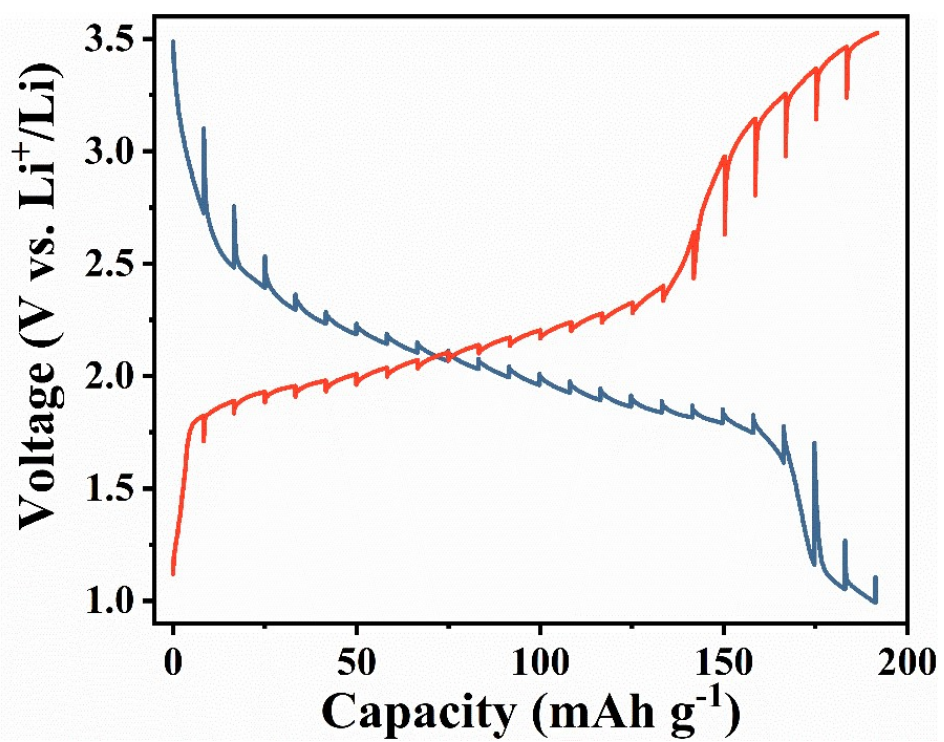
Figure S11. Charge-discharge curves for GITT tests. The test is performed after 30 activation cycles at 2 mV s^{-1}.
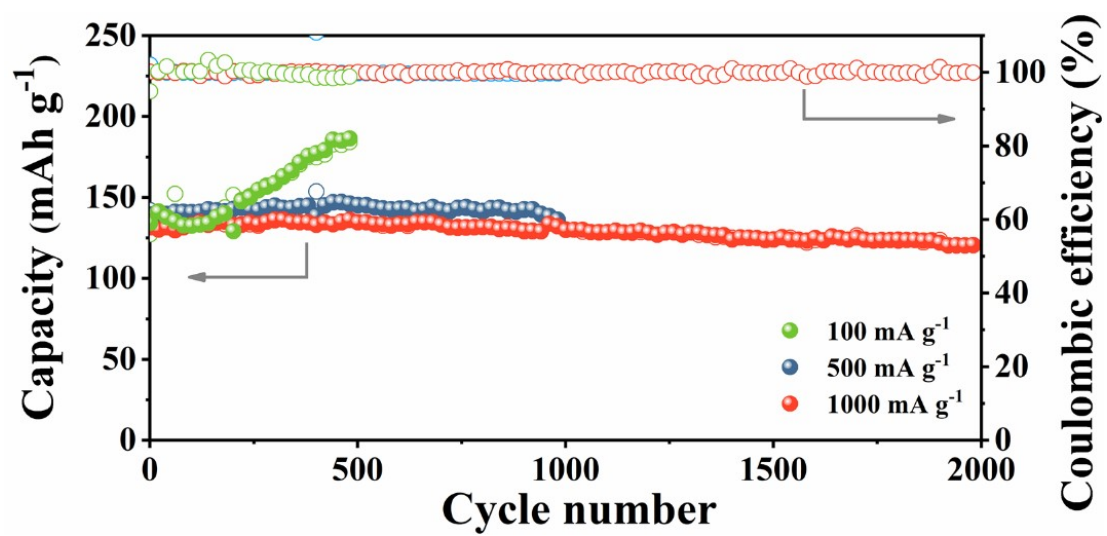
Figure S12. Long-term cycling performance of PSQ cathode at 100, 500 and 1000 mA g^{-1}.
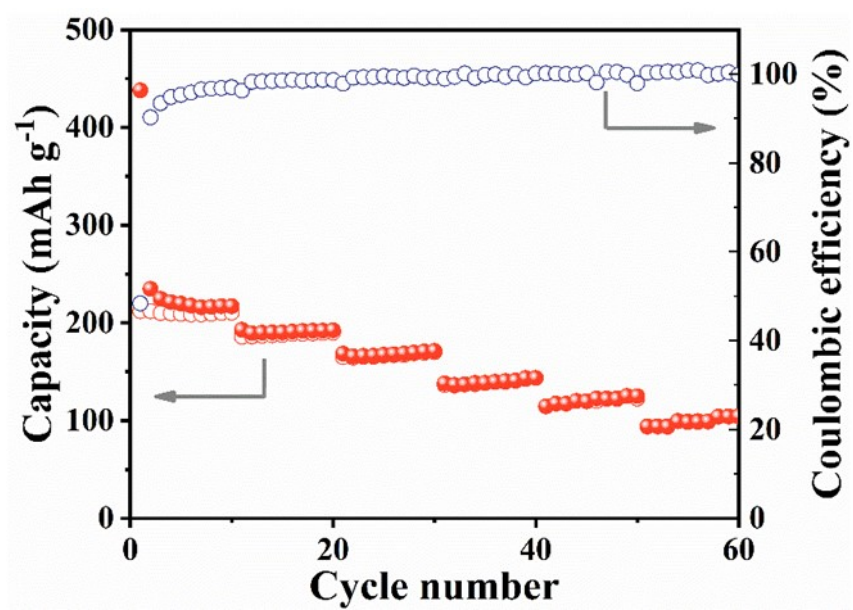
Figure S13. The rate performance of conductive carbon in the PSQ anode at various current rates (from 50 to 2000 mA g^{-1}, voltage range: 0.01-3.0 V).
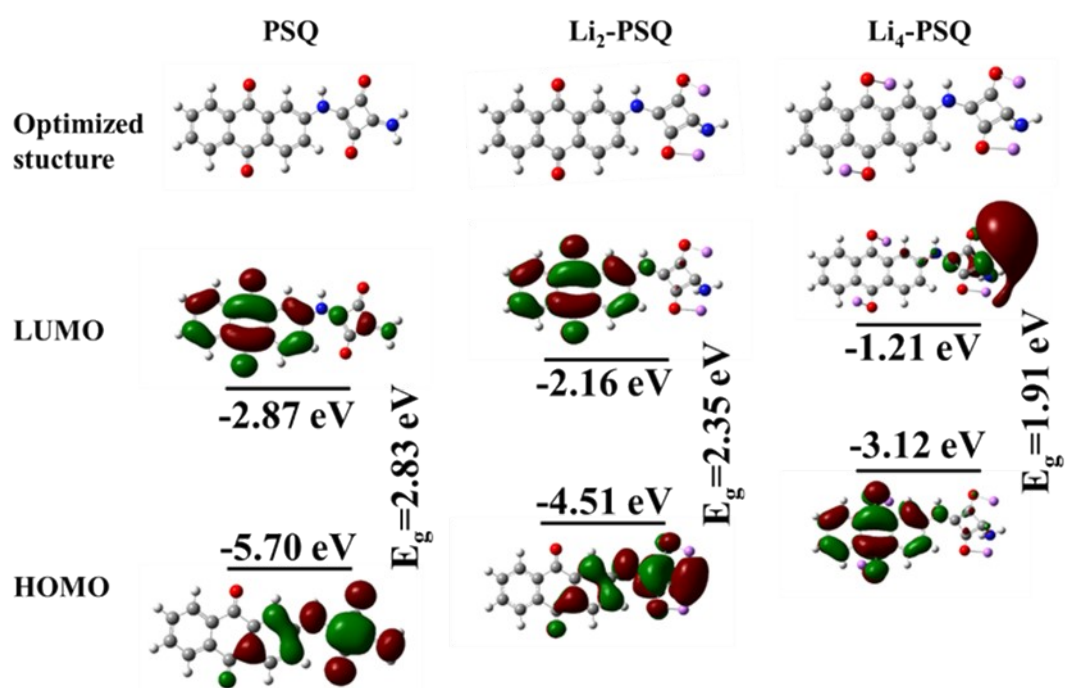
Figure S14. HOMO and LUMO distribution of PSQ in different states.
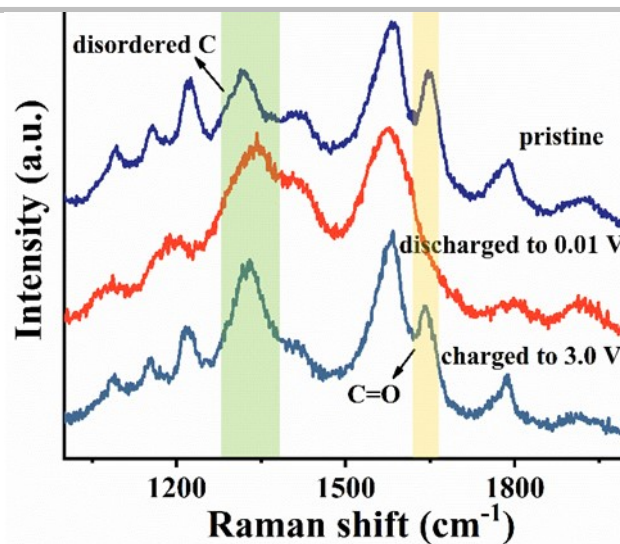
Figure S15. Ex-situ Raman spectra of PSQ anode in different states.
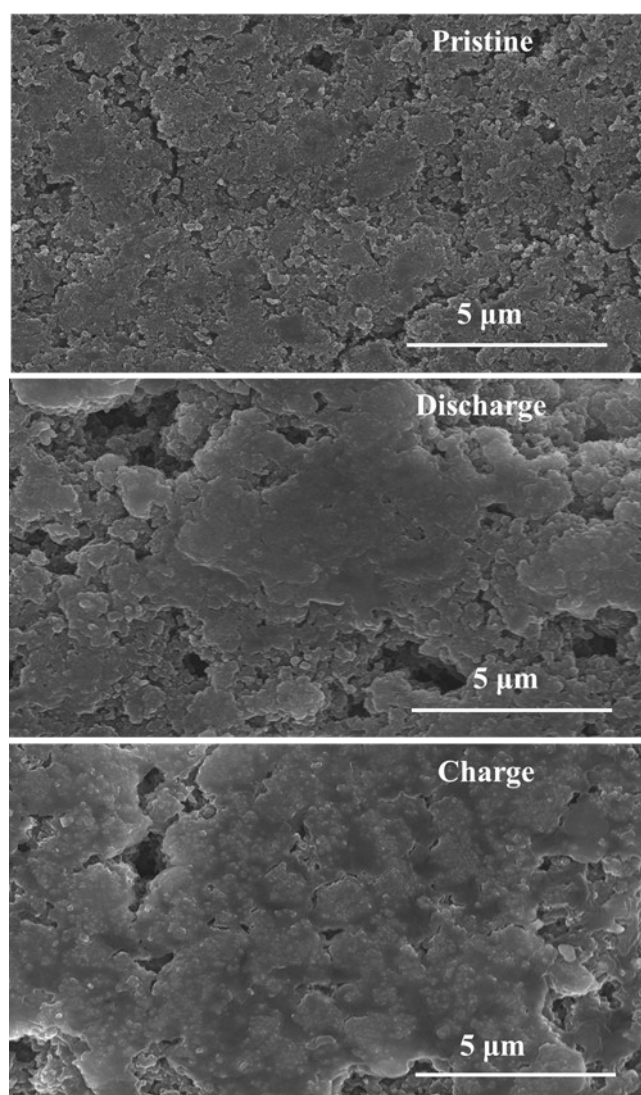
Figure S16. Ex-situ SEM images of the PSQ cathodes in different states at 50 mA g^{-1}.
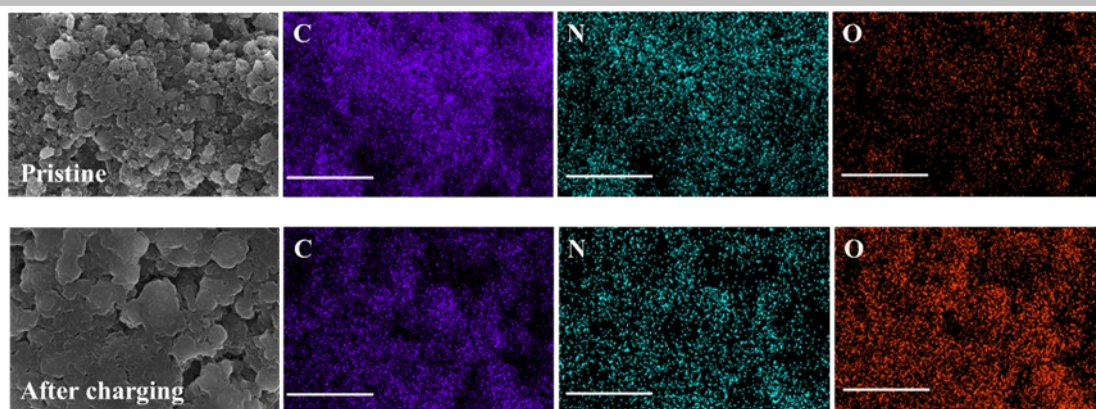
Figure S17. The SEM images and EDS surface distribution images of different elements. (pristine and after 10 cycles, the labelled scale bar is 5 μm)
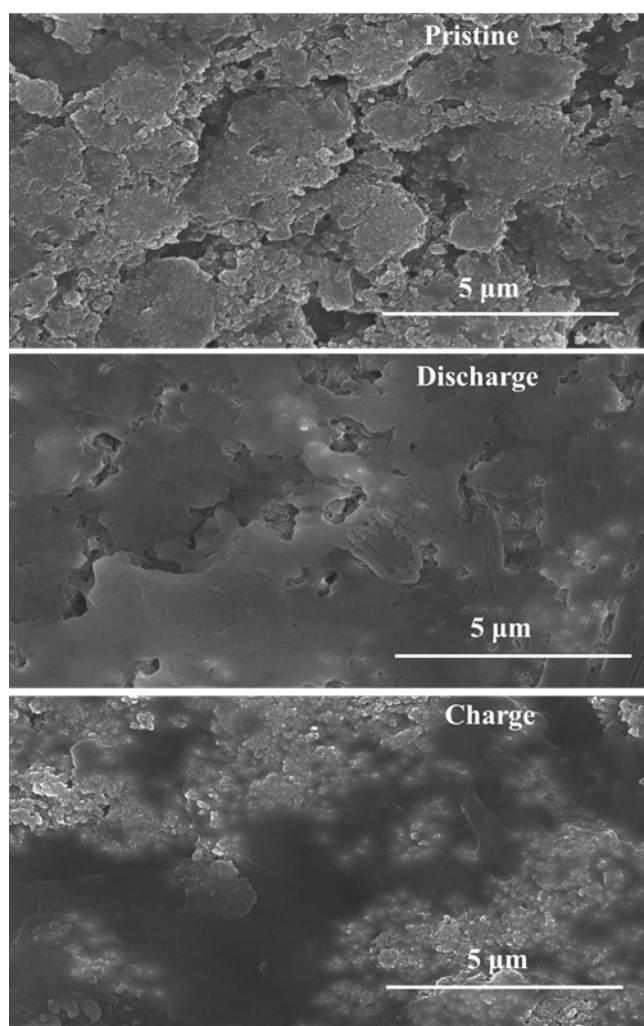
Figure S18. Ex-situ SEM images of the PSQ anode in different states at 100 mA g^{-1}.
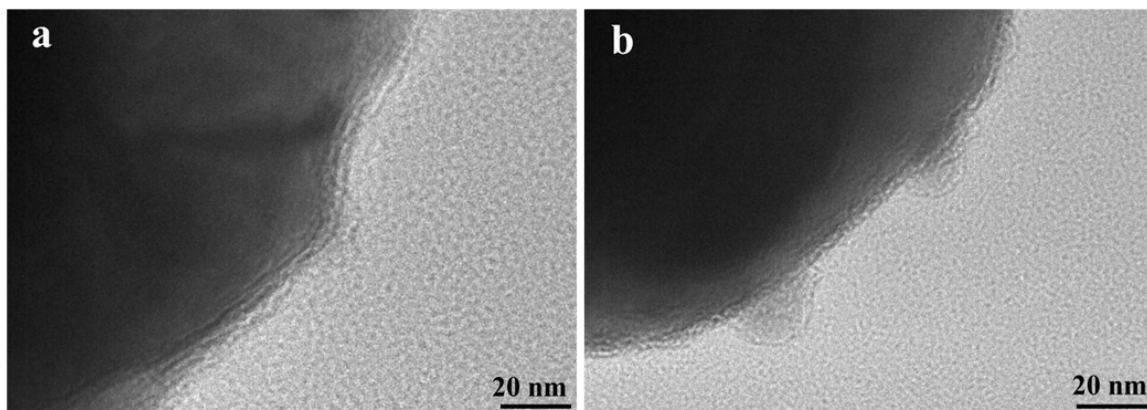
Figure S19. (a) and (b) TEM images of cycled PSQ anode.
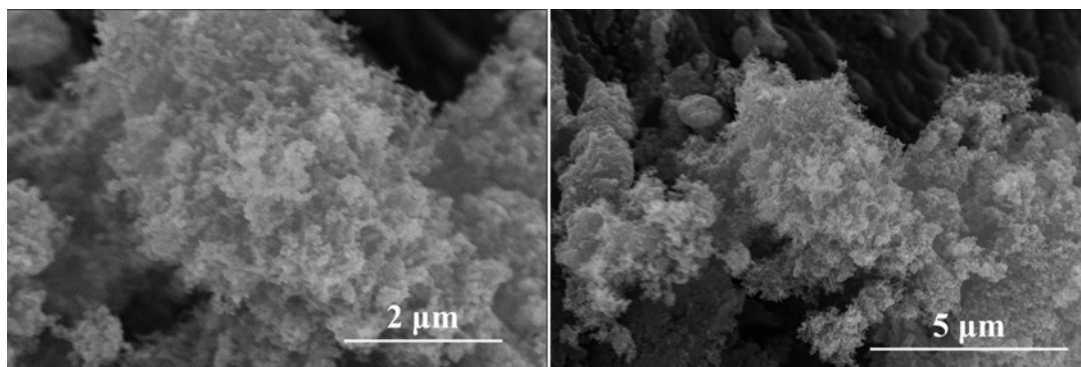
Figure S20. SEM images of PSQ-K.
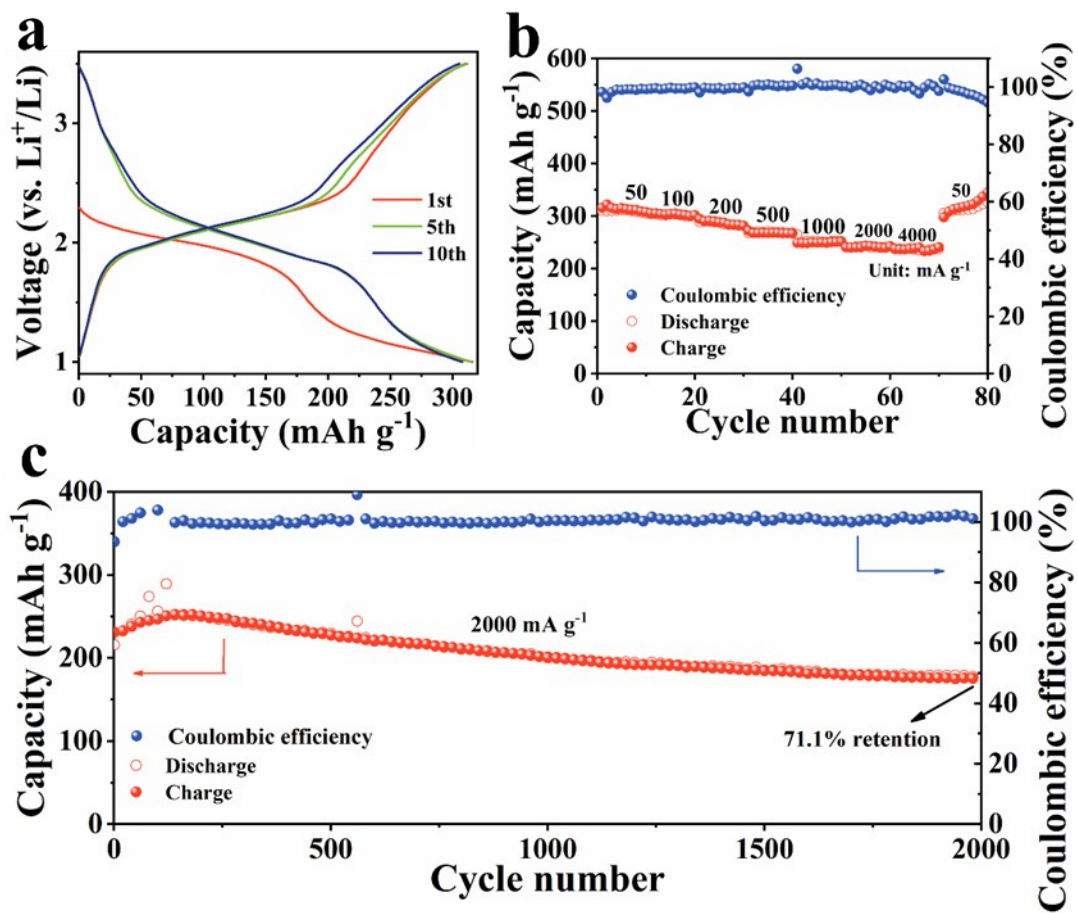
Figure S21. Electrochemical performance of PSQ-K. (a) Charge-discharge profiles. (b) Rate performance. (c) Cycling stability at 2000 mA g^{-1}.
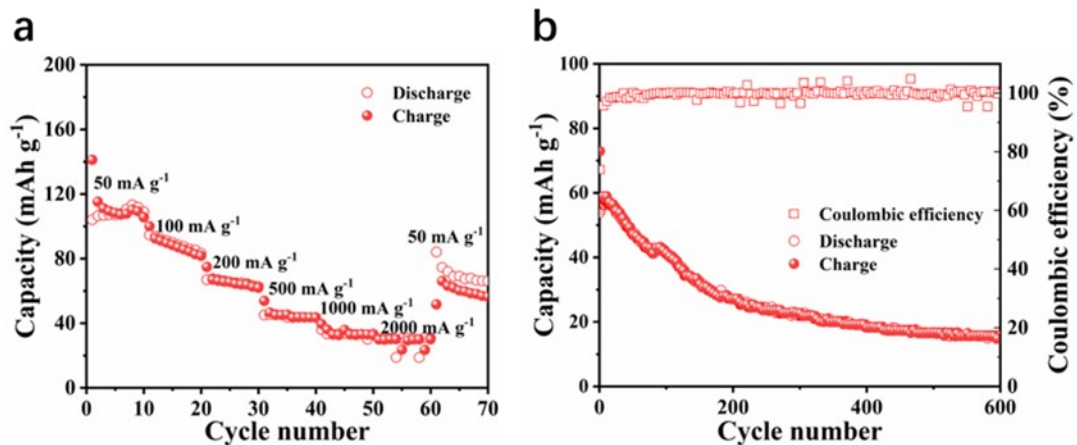
Figure S22. The electrochemical performance of PSQ all-organic battery using 1 M LiPF$_6$ in ethylene carbonate (EC): diethyl carbonate (DEC) (1: 1 v/v).
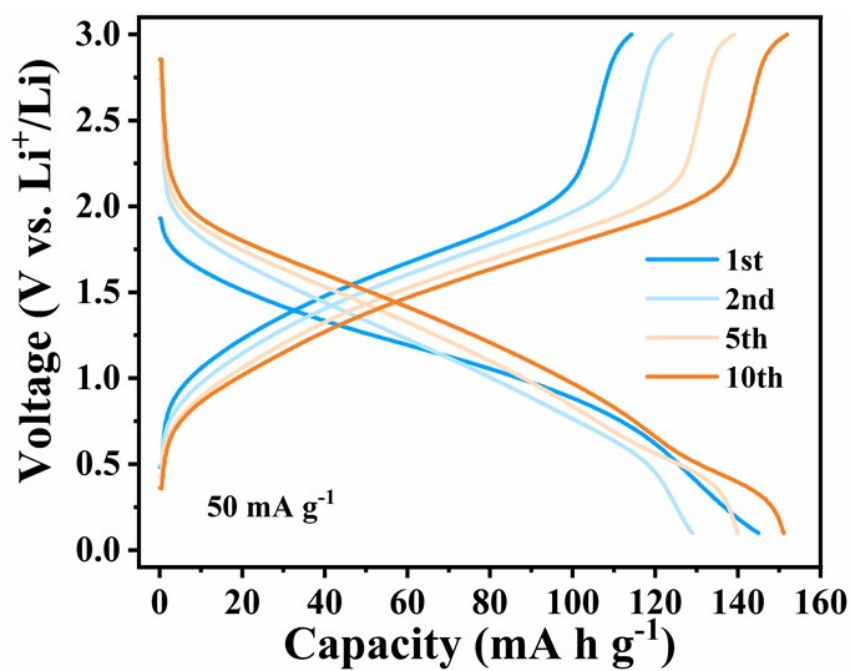
Figure S23. The charge-discharge curves of the PSQ-based all-organic symmetric battery at 50 mA g^{-1} for 10 cycles.
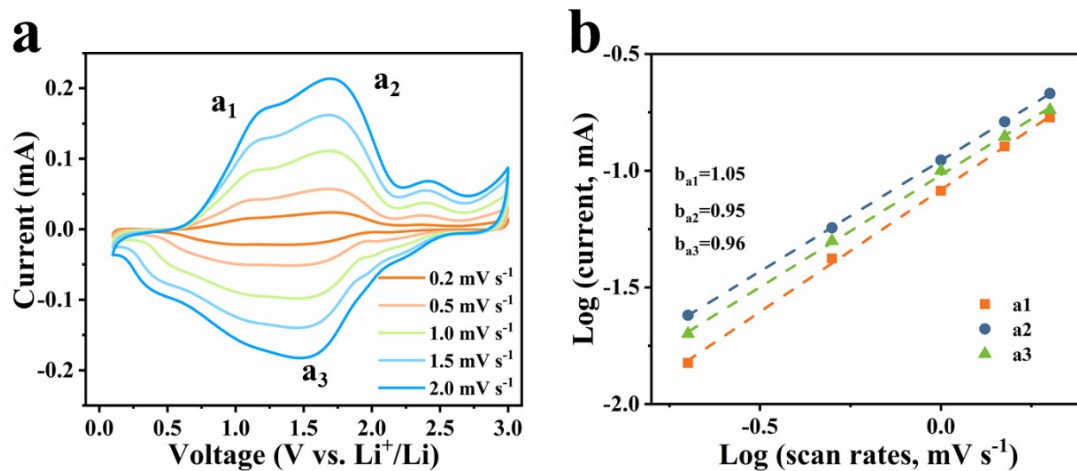
Figure S24. The reaction kinetics study of PSQ all-organic symmetric battery. (a) CV curves at various scan rates from 0.2 to 2 mV s^{-1}. (b) Plots of peak current versus scan rate and the b-values obtained according to i=a v^b.

Table S1. Optimized configuration of monomers.

Optimized configuration	Top view	Side view
2,6-DAQ		
SQ		
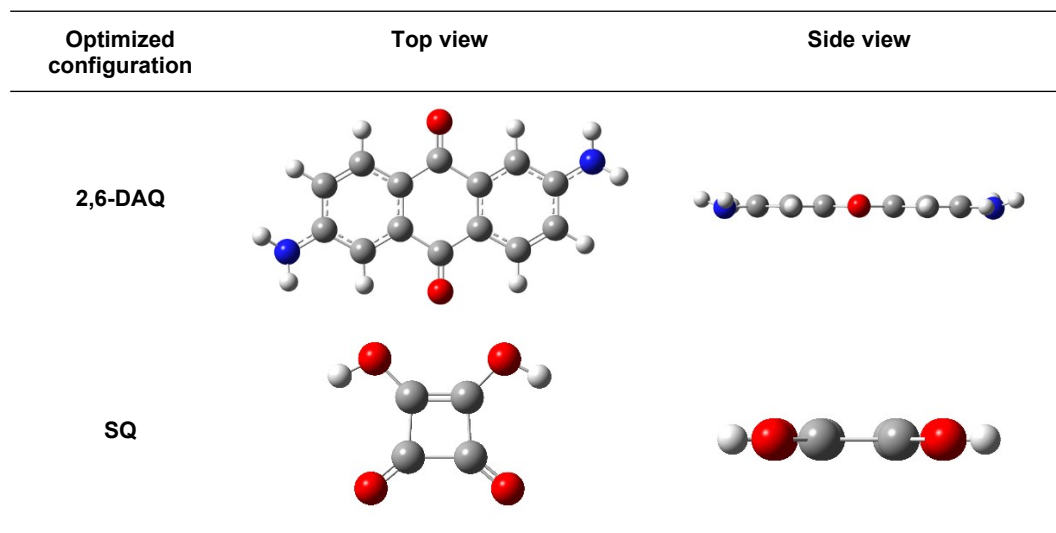
Table S2. Elemental analysis of PSQ.

		C%	H%	N%
PSQ	Theoretical value	68.36	2.55	8.86
	Experimental value	64.52	4.07	8.25

Table S3. Comprehensive electrochemical performance comparison for reported all-organic batteries (corresponding to Figure 6d in manuscript).

Cathode /anode	Electeode composition (active material: conductive carbon : binder)	Reversible Capacity [1] （mAh g^{-1}）	Rate capacity retention	Cycle number @ current density	Cycling capacity retention	Discharging voltage	Rate magnification times [2]	Ref. no.
Thianthrene/TCAQ	40:55:5	103	32.2%	250 @ 1C	68%	1.35 V	50	1
PDB/PDB	30:50:20	160	22.1%	250 @ 500 mA g^{-1}	68%	1.3 V	50	2
Na$_4$C$_8$H$_2$O$_6$/Na$_4$C$_8$H$_2$O$_6$	65:30:5	147	56.5%	100 @ 19 mA g^{-1}	76%	1.8 V	50	3
PI1/PI1	40:40:20	115	96.9%	1000 @ 1000 mA g^{-1}	94%	0.8 V	20	4
BPPF/BPPF	70:20:10	45	26.2%	1000 @ 1000 mA g^{-1}	90%	1 V	40	5
PTPAn/PNTCDA	45:45:10	90	76.9%	500 @ 5C	83%	1.2 V	100	6
PZDB/PZDB	70:20:10	44	83.3%	200 @ 1C	83%	2.5 V	4	7
PTPAn/PI5	60:30:10	105	54%	100 @ 1C	93%	1.45 V	100	8
3BQ/3BQ	50:40:10	110	17.5%	300 @ 0.2C	35.6%	0.7 V	10	9
PTCDI-DAQ/Li$_4$TP	60:30:10	200	45.9%	600 @ 100 mA g^{-1}	60%	1.37 V	100	10
Poly-BQ1/Poly-BQ1	50:40:10	254	57.9%	400 @ 500 mA g^{-1}	85%	1.1 V	20	11
PSQ/PSQ	**50:40:10**	**152**	**64.9%**	**2500 @ 500 mA g^{-1}**	**97%**	**1.4 V**	**80**	**This work**
				10000 @ 2000 mA g^{-1}	**68.4%**			

Footnotes: (1) The reversible capacity was collected when the selected batteries were tested under a current density of ca. 1C. (2) The rate magnification times were calculated by dividing the high current rate by the low current rate for the rate capacity retention.

References

1. A. Wild, M. Strumpf, B. Häupler, M. D. Hager, U. S. Schubert, *Adv. Energy Mater.,* 2017, **7**, 1601415.

2. J. Xie, Z. Wang, Z. J. Xu, Q. Zhang, *Adv. Energy Mater.,* 2018, **8**, 1703509.

3. S. Wang, L. Wang, Z. Zhu, Z. Hu, Q. Zhao, J. Chen, *Angew. Chem. Int. Ed.,* 2014, **126**, 6002-6006.

4. N. Casado, D. Mantione, D. Shanmukaraj, D. Mecerreyes, *ChemSusChem,* 2020, **13**, 2464-2470.

5. K. Sakaushi, E. Hosono, G. Nickerl, H. Zhou, S. Kaskel, J. Eckert, *J. Power Sources,* 2014, **245**, 553-556.

6. X. Dong, Z. Guo, Z. Guo, Y. Wang, Y. Xia, *Joule,* 2018, **2**, 902-913.

7. G. Dai, Y. He, Z. Niu, P. He, C. Zhang, Y. Zhao, X. Zhang, H. Zhou, *Angew. Chem. Int. Ed.,* 2019, **58**, 9902-9906.

8. J. Qin, Q. Lan, N. Liu, Y. Zhao, Z. Song, H. Zhan, *Energy Storage Mate*r., 2020, **26**, 585-592.

9. Y. Zhang, Z. Sun, X. Kong, Y. Lin, W. Huang, *J. Mater. Chem. A,* 2021, **9**, 26208-26215.

10. X. Wang, W. Tang, Y. Hu, W. Liu, Y. Yan, L. Xu, C. Fan, *Green Chem.,* 2021, **23**, 6090-6100.

11. Y. Zhao, M. Wu, H. Chen, J. Zhu, J. Liu, Z. Ye, Y. Zhang, H. Zhang, Y. Ma, C. Li, Y. Chen, *Nano Energy,* 2021, **86**, 106055.